

# BEAM DYNAMICS STUDIES IN A TESLA POSITRON PRE-ACCELERATOR

V.A. Moiseev, V.V. Paramonov, K. Flöttmann<sup>1</sup>  
Institute for Nuclear Research, Russian Academy of Sciences  
60th October Anniversary Prospect, 7a  
Moscow, 117312, Russia, e-mail: moiseev@al20.inr.troitsk.ru  
<sup>1</sup>DESY, Hamburg, Germany

The TESLA linear collider is based on superconducting accelerating cavities. Behind the positron production target normal conducting cavities have to be used in order to cope with high particle losses and with focusing solenoid surrounding the cavities. The main purpose of this pre-accelerator is to provide maximum capture efficiency for the useful part of the totally acceptable positron beam with technically reasonable parameters of the linac. The coupled optimization of the capture optics behind the target and pre-accelerator rf-operation has been carried out. The beam dynamics simulation results as well as the pre-accelerator peculiarities are presented.

PACS numbers: 29.20.Bd

## 1 INTRODUCTION

The Positron Pre-Accelerator (PPA) will be the beginning part of the positron branch of the TESLA 500 GeV electron-positron linear collider with integrated X-ray laser facility [1]. The 250 GeV spent electron beam will be used to produce a positron beam by passing through a wiggler to produce photons, which will hit a thin target to yield the positrons. Since the escaped positrons have a broad distribution of transverse and longitudinal momenta they have to be accelerated in an acceleration section embedded in a solenoid field. The normal conducting cavities have to be used to accelerate a positron beam in order to cope with high particles losses and with focusing solenoid surrounding the cavities. To match the positron beam to the acceptance of the accelerator an Adiabatic Matching Device (AMD) is used [1]. It consists of a tapered solenoid field, which starts with a higher initial field and tapers down adiabatically to the constant end field. After AMD the positron beam should be captured, pre-accelerated to ~250 MeV in the PPA linac, transported to the superconducting linac, accelerated to ~5 GeV and injected into the Damping Ring (DR).

The general AMD and PPA purpose is to form the positron beam with a maximum number of particles acceptable to further use with technically reasonable parameters of the linac. The DR requirements [1] permit to form the parameters for the useful part of  $e^+$  beam at the PPA output energy of (250÷300) MeV as follows:

- for longitudinal phase space an energy spread has to be  $\Delta W/W_f \leq \pm 6\%$  and a phase spread  $\Delta\phi \leq \pm 7.5^\circ$  for the PPA rf-frequency of 1.3 GHz;
- for transverse phase space the normalized emittances have to satisfy the following conditions:  $\epsilon_x \leq 0.036$  m,  $\epsilon_y \leq 0.036$  m and  $\epsilon_x + \epsilon_y \leq 0.048$  m.

## 2 PPA DESIGN

The general PPA scheme is shown in Fig. 1. The scientific and technical details of the design are presented in papers [2] and [3]. The PPA is a standing wave normal conducting linac. Its first part consists of the four Accelerating Cavities (AC) embedded in a focusing solenoid. The first two ACs have a high accelerating gradient (< 14.5 MV/m) to reduce the bunch

lengthening, whereas the others have a moderate gradient (< 8.5 MV/m) to diminish the rf-power consumption. Each AC is powered by one standard TESLA 10 MW klystron.

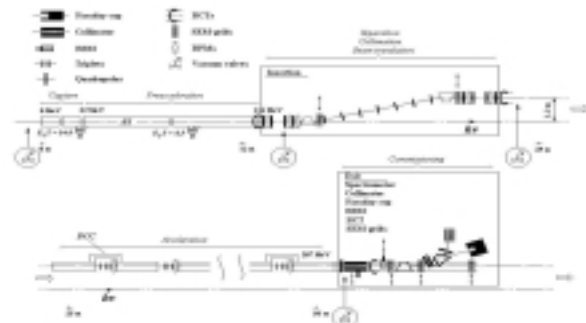


Fig. 1. The general PPA scheme.

Behind the first PPA part (final positron energy ~114 MeV) there is a magnetic insertion to separate the positron and electron beams. Additionally it serves to parallel translation of the PPA axis to a distance of ~(1.0÷1.2) m to pass a powerful photon beam through and to collimate the positron beam. The insertion has a standard achromatic design with two bending dipoles and matching sections on both ends [3].

The second PPA part consists of five ACs with moderate gradient (< 8.5 MV/m). Each AC has two accelerating sections. The quadrupole triplets placed between sections carry out the transverse focusing. Each AC is powered by one 10 MW klystron. The PPA subsystems are described in detail in [2].

## 3 AMD OPTIMIZATION

The AMD is a special solenoid with combined pulsed and time constant magnetic field [4]. Its on axis field is tapered by the law  $B(s) = B_0 / (1 + gs)$ , where  $s$  is the longitudinal coordinate,  $B_0$  is the maximum magnetic field and  $g$  is the taper coefficient. The final AMD field is equal to the constant magnetic field of the PPA solenoid. Depending on initial positron distribution, AMD parameters ( $B_0$  and  $g$ ), solenoid magnetic field and technical reasons there is an optimum of the positron capture efficiency. The reasonable value for  $B_0$  is determined as 6 T and the phase space distributions of the positrons and electrons emitted from the target have

been preliminary defined [4]. The coupled optimization of AMD and PPA in dependence of taper coefficient  $g$ , final AMD field  $B_{sol}$  (or PPA solenoid field) and entering length  $L_{ins}$  of the PPA first AC into the AMD was carried out [3]. In Fig. 2 the positron capture efficiency (left) in % and PPA output beam energy (right) in MeV levels are presented in dependence from the parameter  $g$  and rf-phase scanning in the first AC. There is an optimum for the AMD tapered parameter  $g$ .

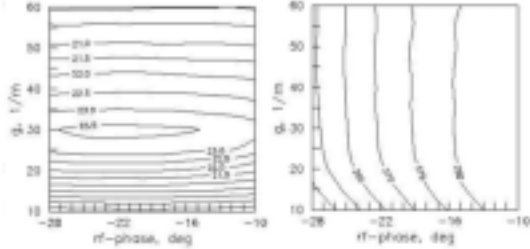


Fig. 2. Positron capture efficiency and output beam energy levels for  $B_{sol}=0.22$  T and  $L_{ins}=0$  m.

In Fig. 3 the positron capture efficiency and PPA output beam energy levels are presented in dependence from the AMD final magnetic field  $B_{sol}$ . The higher final AMD magnetic field is better. However from some value of  $B_{sol}$  the growth rate for the capture efficiency slows down essentially. It results from the PPA acceptance exceeding over the transverse emittance requirement for positron beam.

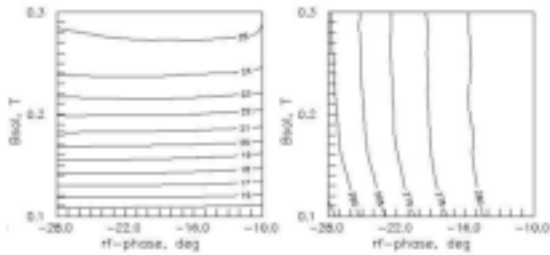


Fig. 3. Positron capture efficiency and output beam energy levels for  $g=33$  m<sup>-1</sup> and  $L_{ins}=0$  m.

In Fig. 4 the positron capture efficiency and PPA output beam energy levels are presented in dependence from the entering length  $L_{ins}$  of the first AC into the AMD. It should be pointed that the evident optimum wasn't reached for the capture efficiency, which has a higher growth rate with  $L_{ins}$  increasing. It results from the bunch lengthening reduction in the AMD. However, in this case, the particle losses are increased in the first high gradient ACs that can lead to technical problems.

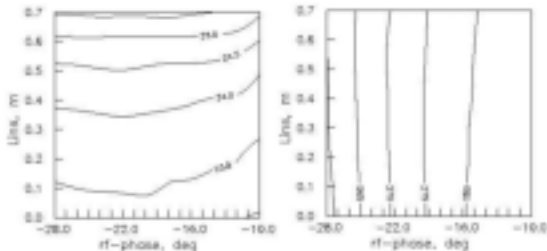


Fig. 4. Positron capture efficiency and output beam energy levels for  $g=33$  m<sup>-1</sup> and  $B_{sol}=0.22$  T.

Analyzing the simulation results and due to the technical reasons the followed parameters were recommended [3]: AMD tapered parameter  $g=29.5$  m; AMD final magnetic field  $B_{sol}=0.22$  T; entering parameter  $L_{ins} \sim 60$ cm (total AMD length is  $\sim 89$  cm).

## 4 PARTICLE LOSSES

A histogram of positron and electron losses in each element of the PPA beginning is presented in Fig. 5 with respect to the total number of positrons and electrons emerging from the target.

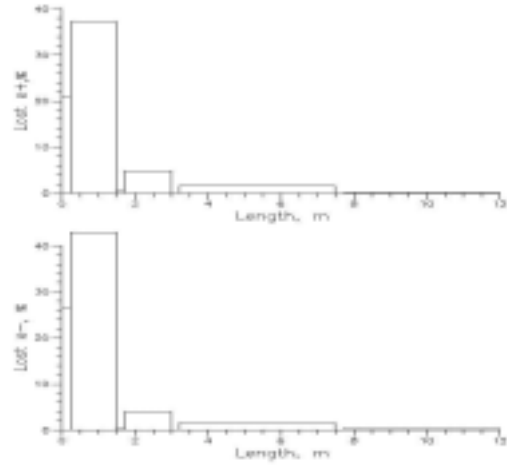


Fig. 5. Particle loss distribution along the first PPA part.

The first column is the particle losses in the AMD. About 65% of the incoming positrons and 76% of the electrons will be lost in the AMD and in the first four ACs resulting in an additional heating.

The total positron losses in the separator are estimated as  $\sim 8.4\%$  of the incoming  $e^+$  beam, composing from the particles with a large momentum deviation. Behind the first dipole of the separator a dump is foreseen which can handle the  $e^-$  power of  $(12 \div 15)$  kW.

The positron losses in the second PPA part are negligible and its value is mainly determined by matching between separator and PPA second part.

## 5 PARTICLE ENERGY CONSUMPTION

The particle dynamics permits to estimate the beam loading effect for each AC. A time depended energy extraction from the first four ACs is shown in Fig. 6.

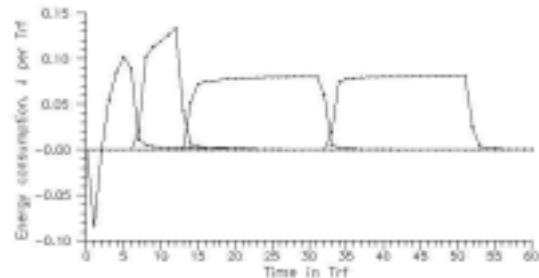


Fig. 6. Time depended energy extraction from the first four ACs.

There is no essential integral consumption of the energy stored in the first AC due to the energy exchange of cavity-accelerated particles and decelerated particles-cavity. The accelerated particles are mainly positrons while the decelerated particles are mainly electrons. Moreover, due to this effect, the first two high gradient ACs operate with a low beam loading, whereas the downstream moderate gradient ACs operate with an approximately constant high integral beam loading.

In the PPA second part ACs have spared positron beam loading [3].

## 6 PARTICLE SEPARATION

In Fig. 7 the longitudinal phase spaces are shown for positron and electron families for situation when acceleration will take place in a solenoid focusing field only. The main feature of this picture is the multibunch trains both for positron and electron beams per one positron production cycle. This process is took place due to the initial bunch lengthening in the AMD and first AC and due to the wide longitudinal momentum spectrum of the initial particle distributions. As was mentioned above it was proposed to move the first AC into the AMD on 60 cm approximately. In this case there is no multibunch structure of the positron beam practically.

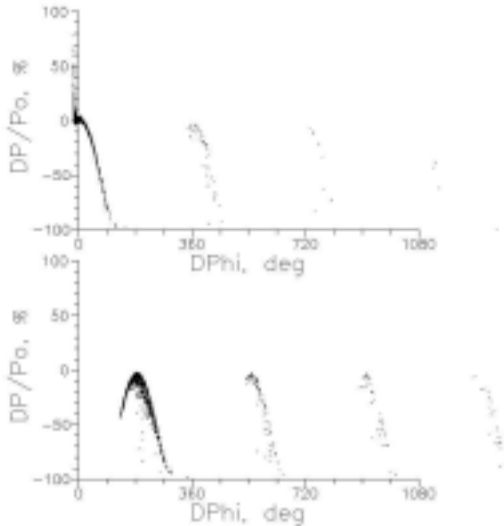


Fig. 7. Longitudinal phase spaces of positrons (top) and electrons (bottom).

It was proposed to place a magnetic insertion behind the first PPA part [2]. Its main purpose is to separate the positrons with electrons and photons. In addition it is possible to use this insertion for collimation and transverse translation of the positron beam.

It was shown [3] that mainly the nonlinear chromatic effects have the dominant role for the final beam quality when a low energy beam with high energy spread has to be transported. For this reason the attractive insertion scheme [2] was disabled and replaced by simpler one [3]. In Figs 8 the positron beam phase space portraits are presented before (a) and after (b) separator respectively.

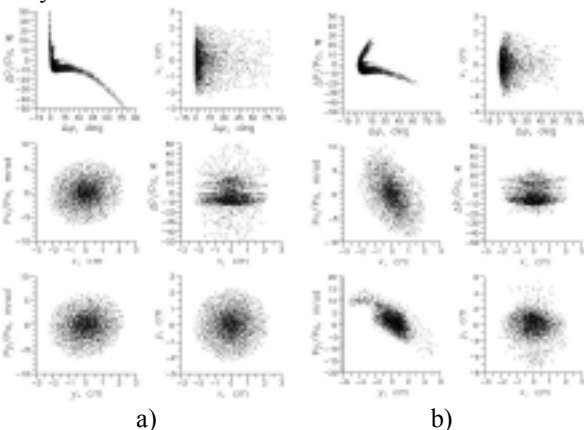


Fig. 8. Phase space portraits of positrons before (a) and after (b) separator.

It is evidence that there are the phase space distortions and particle losses during the positron beam transport across the magnetic insertion. The losses are composed mainly from the particles with a large momentum deviation with respect to the magnetic system central energy. Varying central energy it is possible to adjust the best positron transmission.

## 7 EXIT POSITRON BEAM

After the separator and second acceleration PPA part the positron beam has practically a single bunch structure (Fig. 9) instead of a multibunch structure before the magnetic insertion (Fig. 7). The first  $e^+$  bunch includes  $\sim 99.3\%$  of the total positron number.

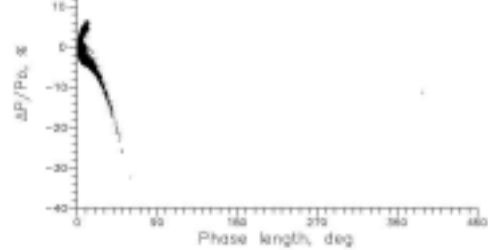


Fig. 9. Longitudinal phase space of positrons at the exit of the PPA.

The final phase space portraits at the PPA exit are shown in Fig. 10. In the first picture the acceptable region for further acceleration is marked by rectangle.

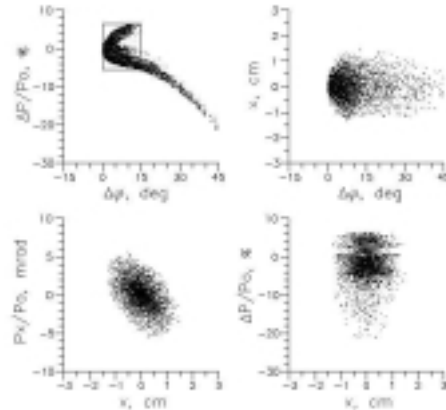


Fig. 10. Phase space portraits of positrons at the exit of PPA.

## 8 CONCLUSIONS

The final result of the beam dynamics studies was the proposal of the conceptual design of a PPA for the TESLA linear collider [2, 3] with output beam energy  $\sim 287$  MeV and positron capture efficiency  $\sim 21.3\%$ .

## REFERENCES

1. *Conceptual Design of a 500 GeV  $e^+e^-$  Linear Collider with Integrated X-ray Laser Facility*, DESY 1997-048, 1997.
2. *Conceptual design of a Positron Pre-Accelerator for the TESLA Linear Collider*, TESLA 99-14, DESY, 1999.
3. *Conceptual Design of a Positron Injector for the TESLA Linear Collider*, TESLA 2000-12, DESY 2000.
4. K.Flöttmann. *Investigations Toward the Development of Polarized and Unpolarized High Intensity Positron Sources for Linear Colliders*, DESY 93-161, 1993.